Article

Adaptive Joint Sigma-Point Kalman Filtering for Lithium-Ion Battery Parameters and State-of-Charge Estimation

Houda Bouchareb [1,*] , Khadija Saqli [1], Nacer Kouider M'sirdi [2] and Mohammed Oudghiri Bentaie [1]

1 LISA Laboratory, Faculty of Science and Technology, Sidi Mohamed Ben Abdellah University, Fez 30000, Morocco; khadija.saqli@usmba.ac.ma (K.S.); oudghiri.ensafes@gmail.com (M.O.B.)
2 HyRES Lab, LIS-SASV, Aix Marseille University–Université de Toulon, 13399 Marseille, France; kouider-nacer.msirdi@lis-lab.fr
* Correspondence: houda.bouchareb@usmba.ac.ma; Tel.: +212-619343566

Abstract: Precise modeling and state of charge (SoC) estimation of a lithium-ion battery (LIB) are crucial for the safety and longevity of battery systems in electric vehicles. Traditional methods often fail to adapt to the dynamic, nonlinear, and time-varying behavior of LIBs under different operating conditions. In this paper, an advanced joint estimation approach of the model parameters and SoC is proposed utilizing an enhanced Sigma Point Kalman Filter (SPKF). Based on the second-order equivalent circuit model (2RC-ECM), the proposed approach was compared to the two most widely used methods for simultaneously estimating the model parameters and SoC, including a hybrid recursive least square (RLS)-extended Kalman filter (EKF) method, and simple joint SPKF. The proposed adaptive joint SPKF (ASPKF) method addresses the limitations of both the RLS+EKF and simple joint SPKF, especially under dynamic operating conditions. By dynamically adjusting to changes in the battery's characteristics, the method significantly enhances model accuracy and performance. The results demonstrate the robustness, computational efficiency, and reliability of the proposed ASPKF approach compared to traditional methods, making it an ideal solution for battery management systems (BMS) in modern EVs.

Keywords: lithium-ion batteries; battery modeling; joint estimation; Adaptive Sigma Point Kalman Filter; state of charge estimation

1. Introduction

In recent years, the need to reduce greenhouse gas emissions and mitigate climate change side effects has mainly contributed to a large shift from internal combustion engine vehicles (ICEVs) to electric vehicles (EVs) [1]. According to the International Energy Agency (IEA) projections, the global fleet of light-duty electric vehicles will grow from around 10 million in 2021 to 124–199 million EVs in 2030 and is expected to reach 970–1940 million EVs by 2050 [2]. As a result, the booming EV market directly impacts the demand for batteries as a key component of EVs.

Due to their high energy density, long cycle life, low self-discharge rate, and wide temperature range, lithium-ion batteries (LIBs) have emerged as the most reliable energy storage system for EVs [3–5]. They are usually connected in series and parallel configurations to achieve the specific power and capacity required by the target application. As the number of connected batteries grows, the system becomes more complex and can adversely affect the performance and safety of the LIB [6]. Additionally, LIBs can be hazardous if improperly handled since they contain combustible material and oxidizing agents [7]. Therefore, the integration of a sophisticated battery management system (BMS) is essential to track the LIB's critical states which include the battery state of charge (SoC) and state of health (SoH), and ensure that the battery operates within its safe operating area (SOA) [6].

Accurate estimation of a battery's internal states requires a sophisticated battery model cable of capturing the LIB dynamic behavior based on external parameters. The

accuracy of the battery model directly influences the battery's overall performance and safety. Three predominant approaches have emerged in literature: electrochemical battery models (EMs) [8,9], equivalent circuit models (ECMs) [10,11] and data-driven battery models [12,13]. ECMs are widely preferred over electrochemical and data-driven models due to their balance between accuracy, computational efficiency, and ease of integration into simulation tools and BMS [14]. They also present a large adaptability across different battery types, sizes, and geometries with minimal need for recalibration which makes them a desirable option for real-time BMS applications. An ECM is typically composed of n-RC networks (where n can be 0, 1, 2, or more), consisting of resistors, capacitors, and voltage sources to reflect the static and dynamic characteristics of the battery. However, increasing the number of RC networks makes the model parameters identification and SoC estimation more demanding for the BMS [15,16]. He et al. [17] compared seven battery models and found that the 2RC-ECM performed the best and provided reliable results.

In BMS, the battery SoC is a critical factor that directly influences the battery's performance, longevity, and safety. It reflects the LIB's remaining capacity relative to its total usable capacity. Due to the non-linear, time-varying characteristics and complex electrochemical reactions occuring within the battery, the SoC cannot be measured directly [18]. Instead, an accurate and timely estimation of the SoC is needed. The literature presents diverse methods for SoC estimation, each offering distinct benefits and shortcomings. The most widely used methods include Coulomb counting (CC) methods, open-circuit voltage (OCV) methods, and model-based methods [19–21]. Despite their simplicity and straightforwardness, the CC and OCV methods fail to accurately predict the battery SoC [22,23]. While the former requires precise knowledge of the initial SoC value, the latter method requires strict tests to measure the battery OCV and extract the SoC. On the other hand, model-based methods are widely preferred in the literature for estimating the battery SoC. As the name implies, this estimation category requires establishing a mathematical representation of battery behavior and then applying various algorithms to asses the battery state.

While model-based methods, such as the Kalman Filter (KF) and its variants, have become increasingly popular for estimating the SoC, their performance is significantly affected by the accuracy of the battery model and parameter estimation. For instance, the Extended Kalman Filter (EKF), one of the most widely adopted algorithms, approximates the nonlinear system by linearizing it at each time step [24–26]. However, this approximation can lead to estimation errors, particularly when dealing with highly nonlinear systems like lithium-ion batteries, where parameters such as internal resistance, capacitance, and OCV change dynamically with the SoC, temperature, and operating conditions.

In response to these challenges, more sophisticated filters, such as the Sigma Point Kalman filter (SPKF), have been developed to better capture the nonlinearities of the system without requiring linearization [27,28]. The SPKF uses a set of deterministic points called Sigma points to accurately estimate the state and model parameters by directly propagating these points through the nonlinear system dynamics. This allows the filter to capture the true mean and covariance of the state distribution without the need for linearization, making it more suitable for the highly nonlinear behavior of lithium-ion batteries. The relevance of the SPKF in battery management systems lies in its ability to handle the dynamic variations in battery parameters more effectively, improving the accuracy of SoC estimation and parameter tracking. Despite these advantages, existing SPKF-based approaches may still struggle under rapidly changing operating conditions, as they typically rely on static process and measurement noise covariance matrices, which do not account for real-time variations in the battery system.

To address these shortcomings, the author proposes an advanced joint estimation approach that integrates an adaptive Sigma Point Kalman filter (ASPKF) with a 2RC-ECM. This novel method not only estimates the battery's SoC but also dynamically identifies the battery's model parameters in real time. By incorporating adaptive noise covariance matrices for both the process and measurement models, the ASPKF is able to respond to

the time-varying nature of LIBs and provide more accurate and reliable estimations under varying conditions.

Specifically, our approach adapts the process noise covariance (Q) based on the change in the predicted state variables, such as SoC and model parameters, between consecutive iterations. This allows the filter to capture the dynamic behavior of the battery more effectively. Similarly, the measurement noise covariance (R) is adapted based on the residual between the predicted and measured terminal voltage, ensuring that the filter remains robust even in the presence of measurement uncertainties.

In this paper, the proposed ASPKF method is compared with two commonly used techniques for joint parameter and SoC estimation: the hybrid recursive least square (RLS)-EKF method, and the simple joint SPKF method. The RLS-EKF method, though capable of estimating both the SoC and model parameters, can suffer from instability in highly dynamic environments due to its reliance on linearization. The simple joint SPKF, while better suited for handling non-linearities, lacks the adaptability needed to fully capture the time-varying behavior of lithium-ion batteries.

Through extensive simulations, the author demonstrates that the ASPKF significantly outperforms both the RLS-EKF and the simple SPKF in terms of accuracy, robustness, and computational efficiency. The results show that the ASPKF provides superior SoC estimation results and more accurate parameter identification under a wide range of operating conditions, making it an ideal solution for modern BMS in EVs.

The remainder of the paper is structured as follows. First, the experimental setup is detailed in Section 2, focusing on the use of the 3 Ah LG-HG2 18650 cylindrical LIB, which will serve as the basis for model validation and parameter estimation. Next, the battery modeling approach is discussed in Section 3, where the 2RC-ECM is selected. This model is chosen for its ability to accurately capture both fast and slow dynamic responses of the LIB, making it well-suited for precise SoC and parameter estimation. The paper then introduces the methodology for joint parameters and SoC estimation in Section 4, starting with an overview of the SPKF appraoch. The process of joint sigma-point filtering is explained in detail, highlighting the key steps involved. Furthermore, the author addresses the challenging issues associated with the standard SPKF, such as handling model uncertainties and maintaining filter stability under varying operating conditions. Finally, the results and comparisons of the proposed methods are presented in Section 5. The performance of the hybrid RLS-EKF method and the simple joint SPKF method is compared against the proposed ASPKF method.

2. Experimental Setup

Modeling the battery and estimating its internal parameters and states requires collecting experimental data that represents the battery response under different tests and operating conditions. The experimental data considered in this paper are those of the 3 Ah LG-HG2 18650 cylindrical cell acquired from [29]. The cell's specifications are shown in Table 1.

A series of tests (the four pulse discharge hybrid pulse power characterization (FPD-HPPC) test and four drive cycles) were performed at six different temperatures ($-20\,°C$, $-10\,°C$, $0\,°C$, $10\,°C$, $25\,°C$, $40\,°C$), and the battery was charged after each test at 1 C-rate to 4.2 V, 50 mA cut off, with battery temperature 22 °C or greater. These tests were performed at McMaster University in Hamilton, Ontario, Canada by Dr. Phillip Kollmeyer [29].

Table 1. LG-HG2 18650 cell specification.

Category	Specification
Manufacturer	LG Chemical
Type	Cylindrical
Chemistry	Li[NiMnCo]O2 (H-NMC)/Graphite + SiO
Nominal Voltage	3.6 V
Nominal Capacity	3.0 Ah
Energy Density	240 (Wh/Kg)
Charge	1.5 A, 4.2, 50 mA End-Current (CC-CV) Normal
	4 A, 4.2 V, 100 mA End-Current (CC-CV) Fast
Discharge	2 V End Voltage, 20 A MAX Continuous Current

As shown in Figure 1, the FPD-HPPC test involves subjecting the battery to a series of discharge and charge pulses at varying C-rates to evaluate its dynamic performance across different SoC levels and temperatures. The discharge C-rates are 1 C, 2 C, 4 C, and 6 C, whereas the charge C-rates are 0.5 C, 1 C, 1.5 C, and 2 C. The FPD-HPPC test is performed across a wide range of SoC levels (100%, 95%, 90%, 80%, 70%, 60%, 50%, 40%, 30%, 20%, 15%, 10%, 5%, 2.5%, 0%) to capture the battery's current, voltage, and other dynamic characteristics at each SoC level.
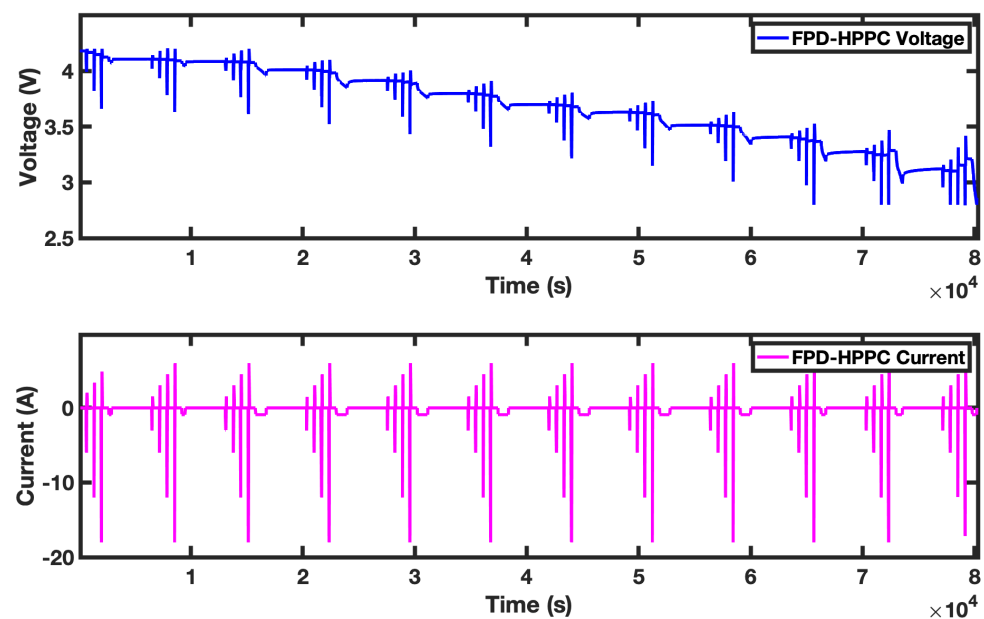
Figure 1. Four pulse discharge hybrid pulse power characterization (FPD-HPPC) current data and battery terminal voltage response.

To assess the battery's performance under real-world driving conditions, drive cycle tests are designed, by simulating power demands typical of electric vehicle operation. In these tests, a series of drive cycles, such as the urban dynamometer driving schedule (UDDS) (see Figure 2), highway fuel economy test (HWFET), LA92, and US06, are performed in sequence. These drive cycles mimic different driving environments, including city driving, highway conditions, and mixed traffic scenarios, generating varying power and energy demands on the battery. These tests are performed at the same six temperatures, ranging from −20 °C to 40 °C.
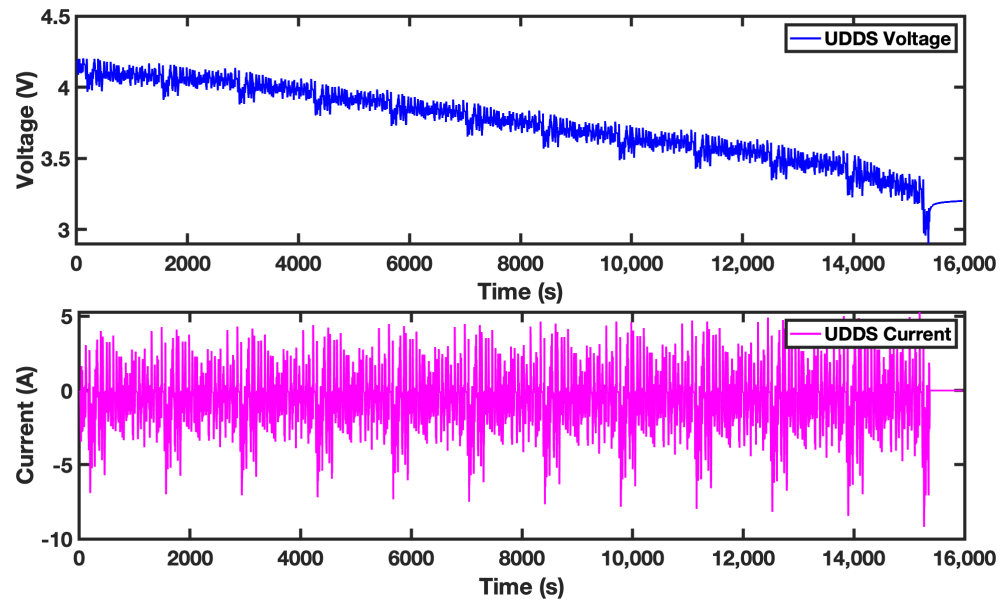
Figure 2. Urban dynamometer driving schedule (UDDS) current data and battery terminal voltage response.

3. Battery Modeling

The 2RC-ECM model, presented in Figure 3, is selected in this paper to simulate the dynamic behavior of the LIB for its accuracy in capturing the battery's fast and slow dynamic responses. The model comprises an ideal voltage source V_{OCV} representing the battery OCV, an internal resistance R_0, and two RC networks (R_1, C_1, R_2 and C_2). The internal resistance (R_0) represents the ohmic losses of the battery, while the two RC networks capture the battery's short-term and long-term dynamic behaviors. The products of R_1, C_1, and R_2, C_2 represent the time constant for the first and second RC pairs, respectively.
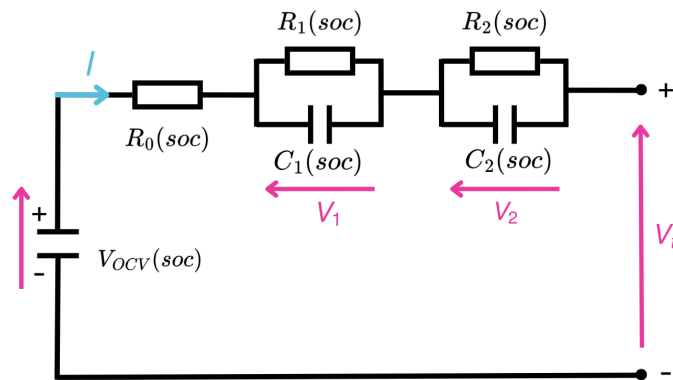

Figure 3. Second order equivalent circuit model (2RC-ECM).

According to Kirchhoff's Voltage law, the governing equations representing the dynamic behavior of the LIB can be expressed as follows

$$
\begin{cases}
\dfrac{dV_1(t)}{dt} & = -\dfrac{V_1(t)}{R_1 C_1} + \dfrac{I}{C_1} \\
\dfrac{dV_2(t)}{dt} & = -\dfrac{V_2(t)}{R_2 C_2} + \dfrac{I}{C_2} \\
V_t(t) & = V_{OCV}(SoC) - V_1(t) - V_2(t) - I(t)R_0
\end{cases}
\tag{1}
$$

where I is the battery current, V_1 is the voltage across the first RC branch and V_2 is the voltage across the second RC branch, V_{ocv} is the battery OCV and V_t is the battery terminal voltage. The 2RC-ECM parameters, R_0, R_1, C_1, R_2 and C_2, are SoC and temperature dependent.

The continuous-time equations of the 2RC-ECM can be discretized to simplify numerical implementation and estimation of the battery's parameters and internal states. The discrete-time state-space representation provides a structured framework for tracking the dynamic response of the battery, which is essential for real-time applications.

The state-space model in discrete form is derived as follows

$$\begin{cases} SoC(k+1) = SoC(k) - \dfrac{\eta \cdot \Delta T}{3600 \cdot Q_{nom}} \cdot I_k \\ V_1(k+1) = exp(\dfrac{-\Delta T}{R_1 \cdot C_1}) \cdot V_1(k) + (1 - exp(\dfrac{-\Delta T}{R_1 \cdot C_1})) \cdot R_1 \cdot I(k) \\ V_2(k+1) = exp(\dfrac{-\Delta T}{R_2 \cdot C_2}) \cdot V_2(k) + (1 - exp(\dfrac{-\Delta T}{R_2 \cdot C_2})) \cdot R_2 \cdot I(k) \\ V_t(k) = V_{OCV}(k) - V_1(k) - V_2(k) - I(k) \cdot R_0 \end{cases} \tag{2}$$

where Q_{nom} is the battery capacity, η is the Coulombic efficiency and ΔT is the sampling time.

4. Joint Parameter and SoC Estimation

The methodologies employed for the joint estimation of model parameters and SoC of the LIB are presented in this section. The effectiveness of the SPKF in managing nonlinear dynamics will be discussed. Subsequently, the joint sigma point filtering process will be explored, and the challenges associated with standard SPKF implementations will be addressed.

4.1. SPKF Overview

The SPKF serves as an effective method to address the intrinsic nonlinearities in battery behavior while jointly estimating the battery model parameters and SoC. Unlike the traditional KF, which assumes linear dynamics, and the EKF, which approximates the system's nonlinearity through first-order linearization, the SPKF provides a more accurate approach by directly working with the nonlinear system model. It achieves this by using a set of carefully selected sample points, known as Sigma Points, to represent the state distribution. These Sigma Points are then passed through the nonlinear dynamics and measurement functions, allowing the SPKF to capture the true behavior of the system without the need for explicit linearization.

The core idea behind the SPKF is to propagate a set of Sigma Points through the nonlinear functions that describe the system and its measurements. At each time step, these Sigma Points are generated based on the current estimate of the state and its covariance, ensuring that their weighted mean and covariance match the current estimate. These points are then passed through the nonlinear system dynamics, resulting in a transformed set of points that represent the predicted state. A similar transformation is applied for the measurement update, allowing the SPKF to update the state estimate based on new observations.

One of the main advantages of the SPKF is its ability to handle strong nonlinearities more effectively than simple KFs. By avoiding linearization, the SPKF provides a more accurate representation of the LIB dynamics where nonlinearities are significant. This makes it ideal for estimating both the battery's SoC and the 2RC-ECM parameters (R_0, R_1, C_1, R_2, C_2).

4.2. Joint Sigma-Point Filtering

According to the literature, the quantities that describe the LIB exist on two-time scales. Battery system states, such as SoC, diffusion voltage, and hysteresis voltage, tend to change quickly. And time-varying parameters of the battery system, such as cell capacity, that fluctuate slowly over time [28]. Estimating both the state and the slow time-varying

cell parameters can be done by combining the cell model state vector with the model parameters and simultaneously estimating the values of this augmented state vector. This approach is known as joint estimation.

Joint estimation makes the battery model more adaptive to real conditions as it allows for simultaneous tracking of both the battery's SoC and model parameters. This leads to more accurate state predictions and performance compared to separate estimation methods, as interdependencies between SoC and parameters are better captured. Despite the increased complexity of matrix operations, SPKF joint estimation methods are straightforward to implement once the state-space model is established.

Combining the state and parameter vectors to form an augmented state is the first step to apply SPKF joint estimation method to the studies battery system. The dynamics may be represented as follows:

$$
\begin{bmatrix} SoC_{k+1} \\ V_{1,k+1} \\ V_{2,k+1} \\ \theta_k \end{bmatrix} = \begin{bmatrix} SoC_k - \dfrac{\eta \cdot \Delta T}{3600 \cdot Q_{nom}} \cdot I_k + w_{k-1} \\ exp(\dfrac{-\Delta T}{R_1 \cdot C_1}) \cdot V_{1,k} + (1 - exp(\dfrac{-\Delta T}{R_1 \cdot C_1})) \cdot R_1 \cdot I_k + w_{k-1} \\ exp(\dfrac{-\Delta T}{R_2 \cdot C_2}) \cdot V_{2,k} + (1 - exp(\dfrac{-\Delta T}{R_2 \cdot C_2})) \cdot R_2 \cdot I_k + w_{k-1} \\ \theta_{k-1} + r_{k-1} \end{bmatrix} \tag{3}
$$

$$
V_t(k) = V_{ocv}(SoC_k) - I_k.R_0 - V_1(k) - V_2(k) + v_k \tag{4}
$$

where Δt is the time step, w_{k-1} is process noise, θ_k represents the battery model parameters at time step k.

With the augmented model of the system state dynamics and parameter dynamics defined, we apply the SPKF method. The state estimation SPKF steps, are presented in Table 2.

4.3. Challenging Issues of Standard SPKF

The SPKF method is widely used in nonlinear control applications and is effective for joint estimation of the battery SoC and parameters. However, the standard SPKF faces several challenges that can affect its accuracy and stability:

- Process and Measurement Noise: For accurate estimation, the SPKF requires prior knowledge of the mean and variance of process noise and measurement noise. Any deviation from the true noise values can degrade the estimation accuracy and even lead to filter divergence. In real-world applications, uncertainties in the physical battery system make it difficult to know the true statistical values of the noises. To address this issue, the SPKF must be adapted to account for unknown or time-varying noise statistics. Considering the statistical value of noises may be time-varying, an adaptive update method for time-varying statistical values should be proposed.

- Positive Definiteness of the Error Covariance Matrix: The error covariance matrix must remain positive definite during the SPKF process to ensure the filter's stability and accuracy. However, due to uncertainties and numerical rounding errors, maintaining the positive definiteness of the matrix can be difficult, which could lead to filter divergence or failure. To solve this, the Cholesky decomposition method is used to decompose the error covariance matrix, ensuring it remains positive definite throughout the estimation process.

In summary, to overcome these drawbacks, an ASPKF method is proposed, which includes additional steps for noise statistics estimation and Cholesky decomposition to ensure stability and robustness in the presence of uncertainties.

Table 2. Summary of the nonlinear sigma-point Kalman filter (SPKF) for joint parameters and states estimation.

State-space model	$$\begin{bmatrix} x_k \\ \theta_k \end{bmatrix} = \begin{bmatrix} f(x_{k-1}, u_{k-1}, w_{k-1}, \theta_{k-1}, r_{k-1}, k-1) \\ \theta_{k-1} + r_{k-1} \end{bmatrix}$$ $$y_k = h(x_k, u_k, v_k, \theta_k, k)$$ where w_k, r_k, and v_k are independent Gaussian noise processes with covariances Σ_w, Σ_r, and Σ_v, respectively. For simplicity, let $X_k = \begin{bmatrix} x_k^T, \theta_k^T \end{bmatrix}^T$, $W_k = \begin{bmatrix} w_k^T, r_k^T \end{bmatrix}^T$, and $\Sigma_W = \mathrm{diag}(\Sigma_w, \Sigma_r)$.
Initialization: for $k = 0$, set	$$\hat{X}_0^+ = \mathbb{E}[X_0]$$ $$\Sigma_{X_0}^+ = \mathbb{E}\left[(X_0 - \hat{X}_0^+)(X_0 - \hat{X}_0^+)^T \right]$$ $$\Sigma_{X,0}^{a,+} = \mathrm{diag}(\Sigma_{X_0}^+, \Sigma_W, \Sigma_v)$$
Computation: for $k = 1, 2, \ldots,$ compute State estimate time update	$$\Sigma_{X_k,0}^{a,+} = \mathrm{diag}(\Sigma_w, \Sigma_r, \Sigma_v)$$ $$\hat{X}_k^{a,-} = \hat{X}_k^{a,+} + \gamma \left[\sqrt{p \Sigma_{X_k}^{a,+}} \quad -\sqrt{p \Sigma_{X_k}^{a,+}} \right]$$ $$X_k^{a,-} = \mathcal{F}(X_{k-1}^{a,+}, u_{k-1}, X_W, X_v, k-1)$$ $$X_{k,i}^{a,-} = \sum_{i=0}^{p} \alpha_i X_{k,i}^{a,-}$$ $$\Sigma_{X_k}^- = \sum_{i=0}^{p} \alpha_i^{(c)} (X_{k,i}^{a,-} - X_{k,i}^-)(X_{k,i}^{a,-} - X_{k,i}^-)^T$$
Output estimate	$$y_k = h(x_k, u_k, v_k, \theta_k, k)$$ $$\hat{y}_k = \sum_{i=0}^{p} \alpha_i^{(m)} y_{k,i}$$ $$\Sigma_{y,k} = \sum_{i=0}^{p} \alpha_i^{(c)} (y_{k,i} - \hat{y}_k)(y_{k,i} - \hat{y}_k)^T$$
Estimator gain matrix	$$L_k = \Sigma_{Xy,k} \Sigma_{y,k}^{-1}$$
State estimate measurement update	$$\hat{X}_k^+ = \hat{X}_k^- + L_k(y_k - \hat{y}_k)$$
Error covariance measurement update	$$\Sigma_{X_k}^+ = \Sigma_{X_k}^- - L_k \Sigma_{y,k} L_k^T$$

5. Results and Discussion

This section presents the results obtained from the experimental validation and analysis of the proposed methodologies for estimating battery parameters and SoC. The validation of the 2RC-ECM model will be detailed, highlighting its effectiveness in accurately representing the battery dynamics. Following this, the performance of the SPKF approach for joint estimation of battery parameters and SoC will be discussed, along with a thorough examination of the ASPKF and its advantages in improving estimation accuracy and robustness.

5.1. 2RC-ECM Model Validation

The battery OCV is extracted for each discharge pulse corresponding to specific SoC points at the sampling intervals of 1, 0.95, 0.9, 0.8, 0.7, 0.6, 0.5, 0.4, 0.3, 0.2, 0.15, 0.1, 0.05, 0.025, and 0. The corresponding voltage data from the FPD-HPPC test shown in Figure 1 is matched to the corresponding SoC values. During the laboratory tests, the SoC is initially calculated using the ampere-hour counting method. For the intermediate points between the predetermined OCV values, linear interpolation is employed, utilizing a polynomial function to derive the voltage values accurately between the known OCV measurements Figure 4. Additionally, the root mean square error (RMSE) between the measured OCV values and the interpolated OCV values is computed to 0.003898 V.

The interpolation function used is a seventh-order polynomial function is presented as follows:

$$V_{ocv}(SoC) = a_1.SoC^7 + a_2.SoC^6 + a_3.SoC^5 +$$
$$a_4.SoC^4 + a_5.SoC^3 + a_6.SoC^2 + a_7.SoC^1 + a_8 \quad (5)$$

Figure 4 illustrates the relationship between the SoC and OCV, highlighting how the OCV varies as a function of SoC.
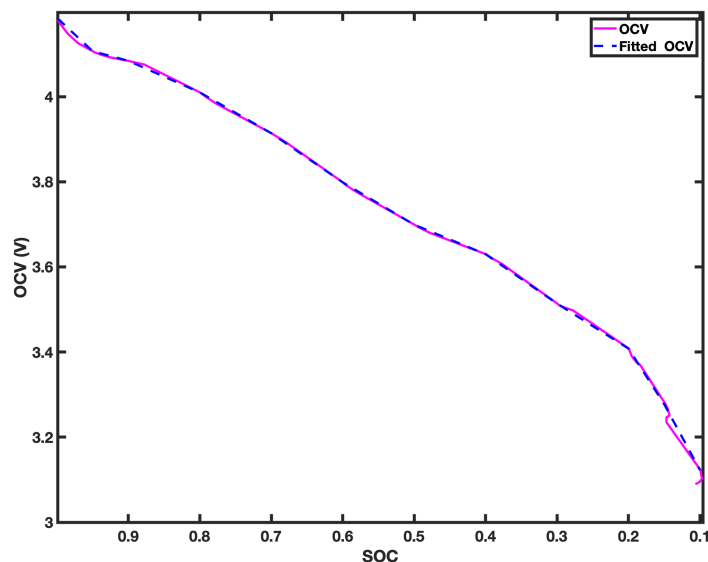
Figure 4. State of charge-open circuit voltage (SOC-OCV) curve.

To validate the 2RC-ECM's performance, the measured and estimated battery terminal voltage under the FDP-HPPC test, UDDS and LA92 drive cycles at 25 °C are illustrated respectively in Figures 5–7. To evaluate the effectiveness of the proposed battery model, the corresponding estimation errors are also plotted.

The voltage error under the FPD-HPPC test is minor with an RMSE equal to 0.0069 V. Similarly, the UDDS test results showed good agreement between the estimated and measured terminal voltages with an RMSE of 0.00208 V.
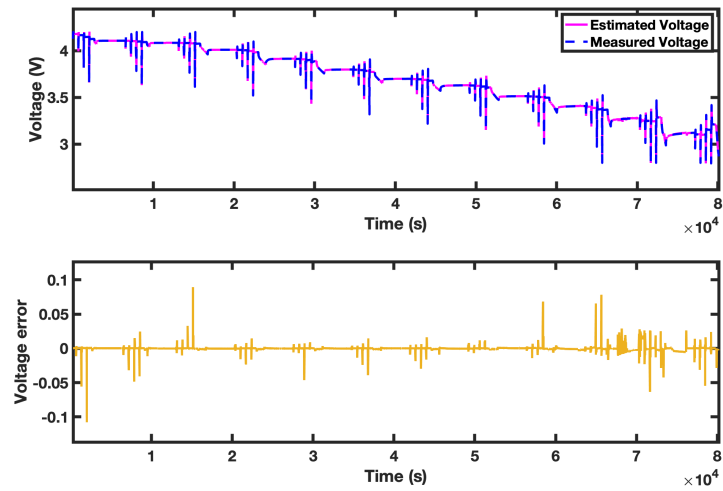
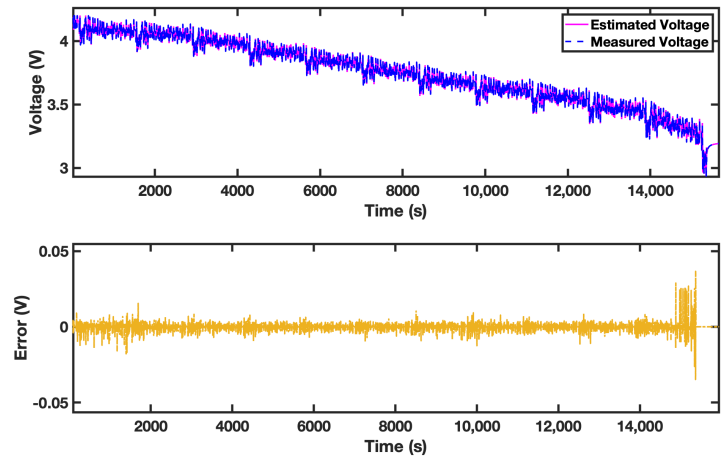**Figure 5.** 2RC-ECM voltage response under FPD-HPPC test at 25 °C.

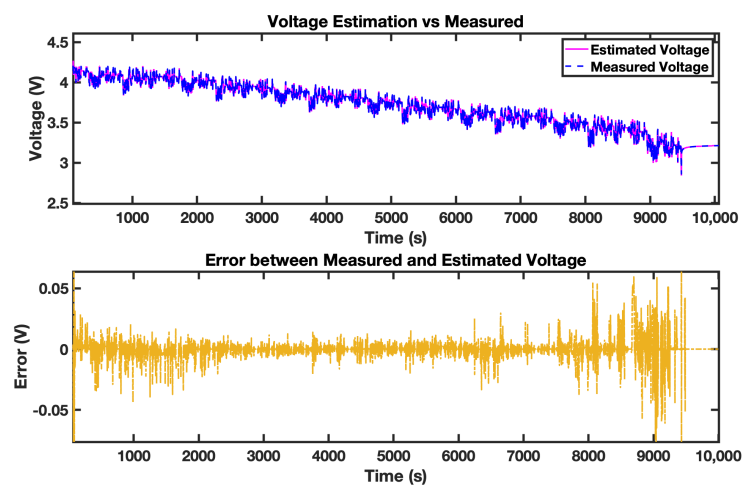**Figure 6.** Measured and estimated battery terminal voltage under UDDS test at 25 °C.

Figure 7. Measured and estimated battery terminal voltage under LA92 test at 25 °C.

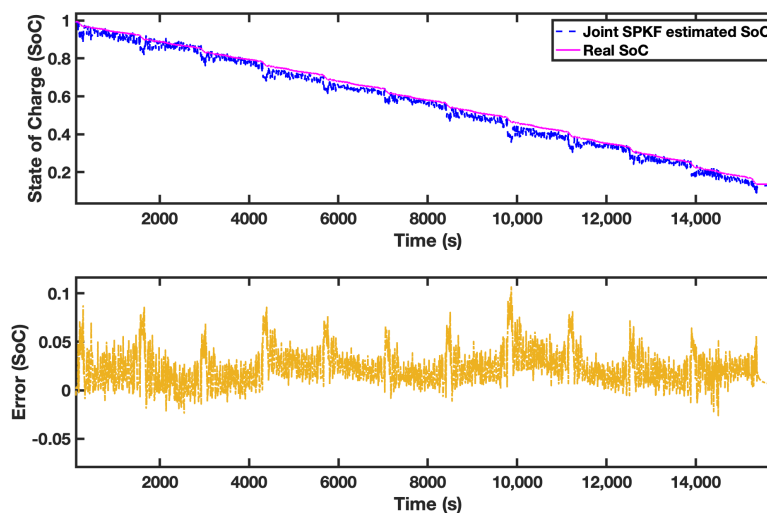*5.2. SPKF-Joint Estimation of Battery Parameters and SoC*

This section presents the results obtained from applying the SPKF for the joint estimation of battery parameters and SoC based on the 2RC-ECM. The methodology was evaluated under various operating conditions to assess its performance and robustness.

The SPKF-joint estimation algorithm, grounded in empirical and experimental values, was rigorously tested under diverse operating scenarios to assess its effectiveness. In this framework, the system state vector is defined as $x = [SoC, V_1, V_2, R_0, R_1, C_1, R_2, C_2]$.

The state covariance matrix P was initialized as a diagonal matrix, reflecting the initial uncertainty associated with the parameters and state, informed by the confidence in the initial estimates. Additionally, the process noise covariance matrix Q represents the uncertainty in the system model, accounting for potential errors or approximations in the dynamics of the system. Finally, the measurement noise covariance R was designed to balance the trust between model measurements and predictions, ensuring optimal filter performance.

To further evaluate the robustness of the proposed method, simulations were conducted under different load profiles, specifically UDDS and LA92. Figure 8 presents the SoC estimation results under the UDDS test at 25 °C. The simple SPKF approach maintained an RMSE of 0.0314%. Additionally, it robustness was quantified with a robustness score of 0.00035511. This demonstrated good accuracy and stability throughout the tests. However, while the computational efficiency of the SPKF, requiring 996.23 s for processing, is satisfactory, there remains potential for improvement in the overall estimation accuracy and robustness. The ASPKF method proposed in this paper aims to enhance these outcomes, addressing dynamic behavior more effectively and ensuring timely updates essential for BMS applications where quick decision-making is critical for performance and safety.

Figure 8. SPKF State of charge estimation under UDDS test at 25 °C.

5.3. Adaptive SPKF Joint Estimation of SoC and Parameters

The proposed ASPKF represents a significant advancement in the real-time estimation of battery SoC and battery model parameters by systematically adapting both process and measurement noise covariances. Recognizing that accurate estimation relies heavily on precise knowledge of noise statistics—often unknown or time-varying in practical applications—the ASPKF dynamically adjusts the process noise covariance (Q) based on observed changes in predicted state variables. This adaptation is achieved by calculating the state change as the difference between the predicted state and the mean of the predicted states, allowing for a direct assessment of how much the state estimates vary. The variance of these state changes informs the updates to Q, which are implemented using the equation:

$$Q = (1 - \alpha) \cdot Q + \alpha \cdot \text{var}(\Delta x_i) \tag{6}$$

where α is the adaptation factor, and $\text{var}(\Delta x_i)$ is the variance of the state change. This technique enables Q to reflect the current dynamics of the battery system, adapting rapidly to sudden shifts while preserving information from prior estimates. Moreover, a regulariza-

tion term is included to ensure that Q does not shrink excessively, maintaining sufficient process noise to account for model uncertainties and variations.

Simultaneously, the ASPKF modifies the measurement noise covariance (R) according to the residuals between predicted and measured voltage. By squaring the voltage residuals—representing the differences between the filter's predictions and actual measurements—this method captures the inherent measurement noise associated with sensor inaccuracies and environmental factors. R is updated using the equation:

$$R = (1 - \alpha) \cdot R + \alpha \cdot \text{var}(v_{residual}) \tag{7}$$

This approach ensures that R is responsive to fluctuations in measurement noise, providing a more accurate representation of the uncertainty in the observations. Regularization is also applied to R to prevent it from diminishing too much, ensuring that the filter retains a realistic estimate of measurement noise even during stable periods. This dual adaptation mechanism enhances the filter's robustness against the uncertainties inherent in battery systems, significantly improving estimation accuracy. By addressing both the process and measurement noise in a systematic manner, the ASPKF mitigates potential filter divergence caused by inaccurate noise estimations, setting a new standard for real-time estimation techniques in BMS.

The efficacy of the proposed ASPKF is evidenced by its performance compared to traditional methods. The RMSE values achieved are 0.0473% for the RLS-EKF method, 0.0314% for the Simple SPKF, and an impressive 0.0281% for the ASPKF, demonstrating a marked improvement in accuracy. Additionally, the Mean Absolute Error (MAE) values also reflect this trend, with 0.0235% for the RLS-EKF, 0.0198% for the SPKF, and 0.0172% for the ASPKF. These MAE values reinforce the significant accuracy advantage provided by the ASPKF. Furthermore, while the computation time for the ASPKF was recorded at 1346.98 s, which is longer than the 734.47 s required by the RLS-EKF and 996.23 s by the SPKF, the significant enhancement in robustness—reflected in a robustness score of 0.00087873 for the ASPKF compared to 0.00057873 and 0.00035511 for the RLS-EKF and Simple SPKF, respectively—underscores the value of the adaptive approach. A detailed overview of the ASPKF is provided in Table 3. Table 4 summarizes the performance metrics of the methods RLS-EKF, SPKF and ASPKF, highlighting their RMSE, MAE, computation time, and robustness.

Robustness, in the context of this study, refers to the algorithm's ability to maintain accurate SoC estimation in the presence of noise and parameter uncertainties. Specifically, the robustness metric evaluates:

- Accuracy in SoC Estimation: The algorithm's capability to preserve precision in estimating SoC despite disturbances, noise, or inaccuracies in the battery model parameters.
- Speed of Convergence: How quickly the filter recovers and converges to an accurate SoC estimation after disturbances or variations in system conditions, such as sensor noise or parameter drift, are introduced.

Table 3. Summary of the Adaptive Sigma-Point Kalman Filter (ASPKF) for joint parameters and states estimation.

State-space model	$$\begin{bmatrix} x_k \\ \theta_k \end{bmatrix} = \begin{bmatrix} f(x_{k-1}, u_{k-1}, w_{k-1}, \theta_{k-1}, r_{k-1}, k-1) \\ \theta_{k-1} + r_{k-1} \end{bmatrix}$$ $$y_k = h(x_k, u_k, v_k, \theta_k, k)$$ where w_k, r_k, and v_k are independent Gaussian noise processes with covariances Σ_w, Σ_r, and Σ_v, respectively. For simplicity, let $X_k = \left[x_k^T, \theta_k^T \right]^T$, $W_k = \left[w_k^T, r_k^T \right]^T$, and $\Sigma_W = \text{diag}(\Sigma_w, \Sigma_r)$.
Initialization: for $k = 0$, set	$$\hat{X}_0^+ = \mathbb{E}[X_0]$$ $$\Sigma_{X_0}^+ = \mathbb{E}[(X_0 - \hat{X}_0^+)(X_0 - \hat{X}_0^+)^T]$$ $$\Sigma_{X,0}^{a,+} = \text{diag}(\Sigma_{X_0}^+, \Sigma_W, \Sigma_v)$$
Computation: for $k = 1, 2, \dots$ State estimate time update	$$\hat{X}_k^{a,+} = \mathbb{E}[\hat{X}_k^a] = \left[(\hat{X}_k^+)^T, \hat{W}^T, \hat{v}^T \right]^T$$ $$\Sigma_{X_k,0}^{a,+} = \text{diag}(\Sigma_w, \Sigma_r, \Sigma_v)$$ $$\hat{X}_k^{a,-} = \hat{X}_k^{a,+} + \gamma \left[\sqrt{p\Sigma_{X_k}^{a,+}}, -\sqrt{p\Sigma_{X_k}^{a,+}} \right]$$ $$X_k^{a,-} = \mathcal{F}(X_{k-1}^{a,+}, u_{k-1}, X_W, X_v, k-1)$$ $$X_{k,i}^{a,-} = \sum_{i=0}^{p} \alpha_i X_{k,i}^{a,-}$$ $$\Sigma_{X_k}^- = \sum_{i=0}^{p} \alpha_i^{(c)} (X_{k,i}^{a,-} - X_{k,i}^-)(X_{k,i}^{a,-} - X_{k,i}^-)^T$$
Process Noise Adaptation	Update Q based on the change in the predicted state variables $$Q = (1 - \alpha) \cdot Q + \alpha \cdot var(\Delta x)$$
Measurement Noise Adaptation	Update R based on the residual between predicted and measured voltage. $$R = (1 - \alpha) \cdot R + \alpha \cdot var(residual_{voltage})$$
Output estimate	$$y_k = h(x_k, u_k, v_k, \theta_k, k)$$ $$\hat{y}_k = \sum_{i=0}^{p} \alpha_i^{(m)} y_{k,i}$$ $$\Sigma_{y,k} = \sum_{i=0}^{p} \alpha_i^{(c)} (y_{k,i} - \hat{y}_k)(y_{k,i} - \hat{y}_k)^T$$
Estimator gain matrix	$$L_k = \Sigma_{Xy,k} \Sigma_{y,k}^{-1}$$
State estimate measurement update	$$\hat{X}_k^+ = \hat{X}_k^- + L_k(y_k - \hat{y}_k)$$
Error covariance measurement update	$$\Sigma_{X_k}^+ = \Sigma_{X_k}^- - L_k \Sigma_{y,k} L_k^T$$

Table 4. Performance comparison in terms of RMSE, MAE, computation time, and robustness for different methods.

Metric	RLS+EKF	Simple SPKF	Adaptive SPKF
RMSE (%)	0.0473	0.0314	0.0281
MAE (%)	0.0235	0.0198	0.0172
Computation Time (s)	734.47	996.23	1346.98
Robustness	0.00035511	0.00057873	0.00087873

By considering both accuracy and convergence speed, this metric assesses the stability and reliability of the algorithm under real-world conditions, including system uncertainties and dynamic changes.

$$Robustness = \frac{1}{ConvergenceTime} \tag{8}$$

To ensure the stability and reliability of the estimation process, the use of Cholesky decomposition maintains the positive definiteness of the error covariance matrix throughout the filtering procedure. By addressing these critical challenges, the proposed ASPKF significantly improves the accuracy and reliability of state and parameter estimations, providing a more effective tool for BMS in electrified vehicles. This advancement not only enhances the operational efficiency of energy storage applications but also contributes to the development of more sophisticated control strategies in the field.

The schematic diagram in Figure 9 illustrates a comparative framework for the joint estimation of battery parameters and SoC using different approaches. At the top, three distinct test datasets—FPD-HPPC test, UDDS test, and LA92 test—provide experimental data, including voltage, current, and SoC measurements. This data is utilized by three methods: the Hybrid RLS-EKF, the simple joint SPKF, and the Adaptive Joint ASPKF. These methods aim to identify the parameters of a 2RC-ECM (R_0, R_1, C_1, R_2, C_2) that depend on SoC and perform a joint estimation of battery SoC. The middle row of the diagram presents the mathematical formulations associated with each method, while the bottom row displays performance comparisons. The plots depict the estimated SoC against the real SoC over time for all methods, highlighting their accuracy. Finally, the bar charts provide a comparison of RMSE, computation time, and robustness, thereby indicating the strengths and weaknesses of each method. The results clearly demonstrate the high accuracy and robustness of the proposed ASPKF, as it consistently achieves lower RMSE values and higher robustness across various test scenarios.

To summarize, Figure 10 compares the performance of the traditional RLS-EKF and joint SPKF methods to the proposed ASPKF. The algorithm takes as input the current load and measured voltage to jointly estimate the model parameters and SoC. The chart demonstrates the effectiveness of the proposed approach in accurately predicting both the SoC and parameters simultaneously, all while maintaining a low computational cost.
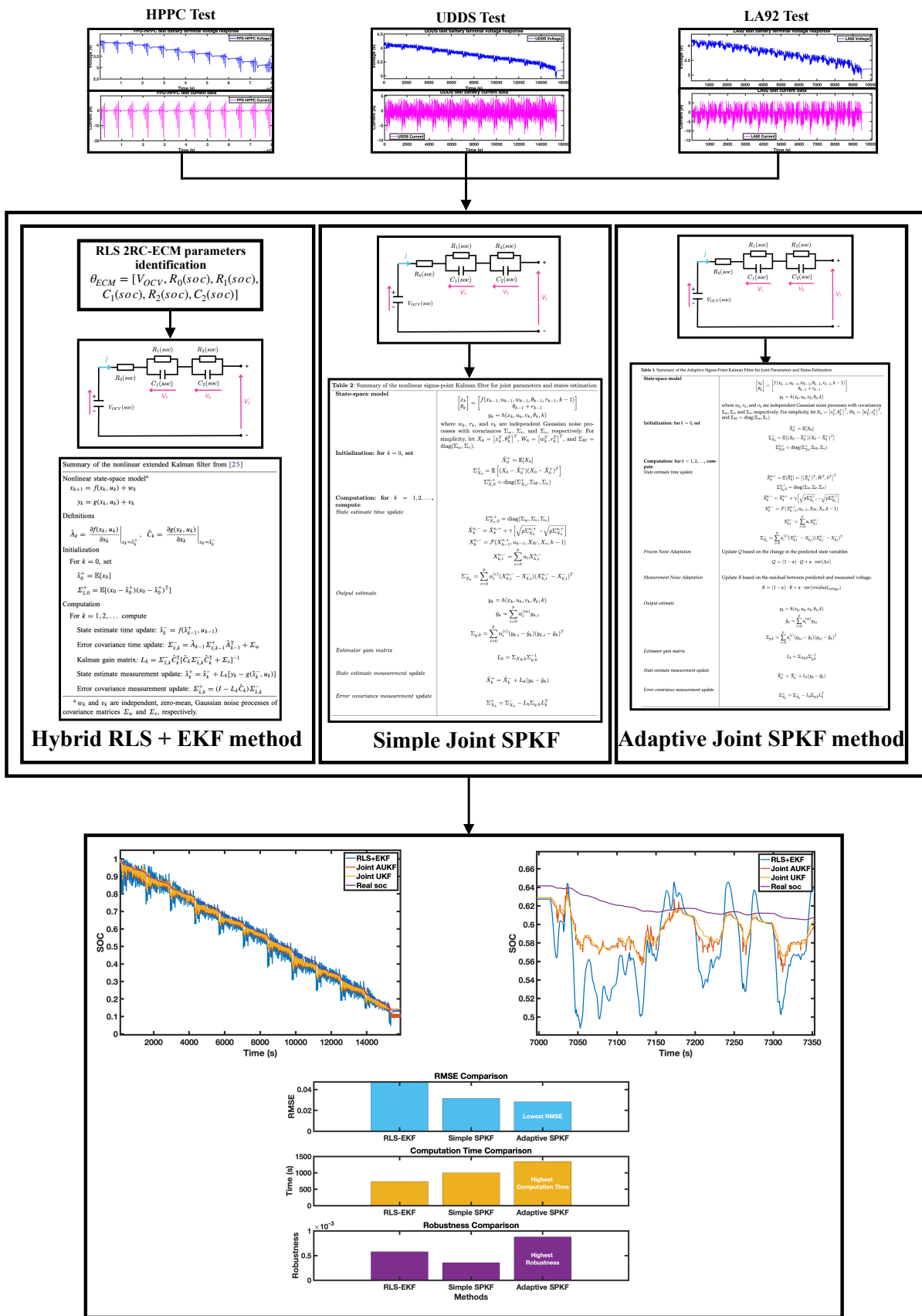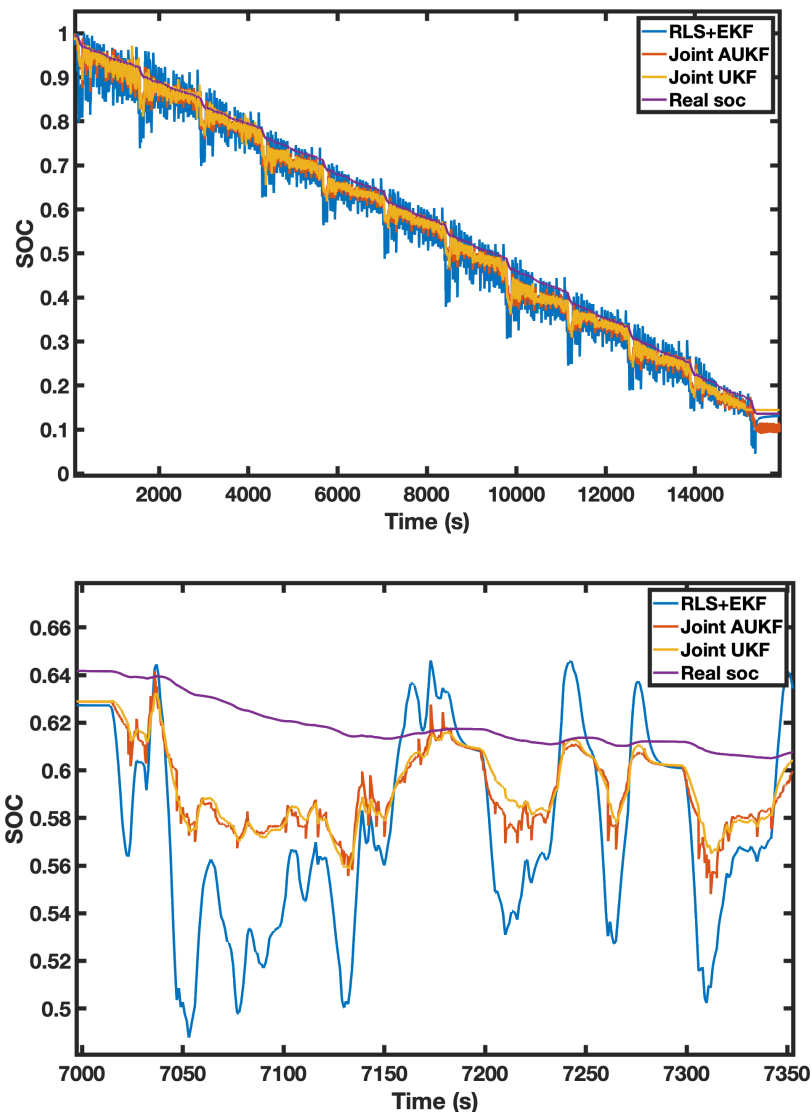
Figure 9. Schematic diagram for the battery parameters and SoC joint estimation.

Figure 10. Comparison between battery SoC estimation results using RLS+EKF/UKF/AUKF under UDDS test at 25 °C.

6. Conclusions

In this study, we presented an advanced joint estimation approach utilizing an ASPKF for the precise modeling and SoC estimation of LIBs. The proposed method effectively addresses the limitations of traditional techniques, such as the hybrid RLS-EKF and the SPKF, particularly under dynamic operating conditions. By integrating an adaptive mechanism for process and measurement noise covariance matrices, the ASPKF demonstrated superior accuracy, robustness, and computational efficiency in estimating both model parameters and SoC.

The author's extensive simulations with the 3 Ah LG-HG2 18650 cylindrical battery validated the effectiveness of the ASPKF [29]. The results indicated that the ASPKF outperforms existing methods with an RMSE of 0.0281%, compared to 0.0314% for the traditional SPKF and 0.0473% for the RLS-EKF method. In terms of computational efficiency, the ASPKF exhibited a computation time of 1346.98 s, while the simple SPKF required 996.23 s, and the RLS-EKF took 734.47 s. Notably, the robustness metrics revealed that the ASPKF achieved the highest value of 0.00087873, surpassing the simple SPKF at 0.00035511 and the RLS-EKF at 0.00057873. These findings highlight the ASPKF's effectiveness in main-

taining performance under varying conditions, making it an ideal solution for modern BMS applications.

Future research will focus on further enhancing the robustness of the ASPKF method, particularly in extreme operating conditions, such as rapid temperature fluctuations and high discharge rates. Additionally, integrating machine learning techniques to predict battery behavior and dynamically adjust filter parameters may significantly improve estimation accuracy. Exploring innovative methodologies, including hybrid approaches that combine data-driven and model-based techniques, as well as applying deep learning algorithms to capture complex relationships in battery data, will be essential for advancing SoC estimation techniques. Continuous improvement in these areas will contribute to optimizing BMS, ensuring the safety, performance, and longevity of lithium-ion batteries in EVs and other applications.

Author Contributions: Conceptualization, H.B.; Methodology, H.B. and N.K.M.; Software, H.B.; Validation, H.B.; Writing—original draft, H.B.; Writing—review & editing, H.B., K.S., N.K.M. and M.O.B.; Supervision, N.K.M. and M.O.B. All authors have read and agreed to the published version of the manuscript.

Data Availability Statement: The data presented in this study are available on request from the corresponding author due to privacy.

Conflicts of Interest: The authors declare no conflicts of interest.

References

1. Xu, C.; Steubing, B.; Hu, M.; Harpprecht, C.; van der Meide, M.; Tukker, A. Future greenhouse gas emissions of automotive lithium-ion battery cell production. *Resour. Conserv. Recycl.* **2022**, *187*, 106606. [CrossRef]
2. IEA. Global EV Outlook, 2022. Available online: https://www.iea.org/data-and-statistics/data-tools/global-ev-data-explorer (accessed on 2 October 2024).
3. Nzereogu, P.; Omah, A.; Ezema, F.; Iwuoha, E.; Nwanya, A. Anode materials for lithium-ion batteries: A review. *Appl. Surf. Sci. Adv.* **2022**, *9*, 100233. [CrossRef]
4. Xu, J.; Cai, X.; Cai, S.; Shao, Y.; Hu, C.; Lu, S.; Ding, S. High-Energy Lithium-Ion Batteries: Recent Progress and a Promising Future in Applications. In *Energy and Environmental Materials*; Wiley: Hoboken, NJ, USA, 2023; pp. 1369–1384. [CrossRef]
5. Duan, J.; Tang, X.; Dai, H.; Yang, Y.; Wu, W.; Wei, X.; Huang, Y. Building Safe Lithium-Ion Batteries for Electric Vehicles: A Review. *Electrochem. Energy Rev.* **2020**, *3*, 1–42. [CrossRef]
6. Chen, Y.; Kang, Y.; Zhao, Y.; Wang, L.; Liu, J.; Li, Y.; Liang, Z.; He, X.; Li, X.; Tavajohi, N.; et al. A review of lithium-ion battery safety concerns: The issues, strategies, and testing standards. *J. Energy Chem.* **2021**, *59*, 83–99. [CrossRef]
7. Kaya, M. State-of-the-art lithium-ion battery recycling technologies. *Circ. Econ.* **2022**, *1*, 100015. [CrossRef]
8. Liu, K.; Gao, Y.; Zhu, C.; Li, K.; Fei, M.; Peng, C.; Zhang, X.; Han, Q.L. Electrochemical modeling and parameterization towards control-oriented management of lithium-ion batteries. *J. Clean. Prod.* **2022**, *124*, 105176. [CrossRef]
9. Marc, D.; Thomas, F.; John, N. Modeling of galvanostatic charge and discharge of the lithium/ polymer/insertion cell. *J. Electrochem. Soc.* **1993**, *140*, 1526–1533. [CrossRef]
10. Hu, X.; Li, S.; Peng, H. A comparative study of equivalent circuit models for Li-ion batteries. *J. Power Sources* **2012**, *198*, 359–367. [CrossRef]
11. Hui, P.; Lian-Jing, M.; Long, G. Parameter identification and state-of-charge estimation approach for enhanced lithium-ion battery equivalent circuit model considering influence of ambient temperatures. *Chin. Phys. B* **2019**, *28*, 108201. [CrossRef]
12. Abu-Seif, M.A.; Abdel-Khalik, A.S.; Hamad, M.S.; Hamdan, E.; Elmalhy, N.A. Data-Driven modeling for Li-ion battery using dynamic mode decomposition. *Alex. Eng. J.* **2022**, *61*, 11277–11290. [CrossRef]
13. Lucaferri, V.; Quercio, M.; Laudani, A.; Fulginei, F.R. A Review on Battery Model-Based and Data-Driven Methods for Battery Management Systems. *Energies* **2023**, *16*, 7807. [CrossRef]
14. Lagnoni, M.; Scarpelli, C.; Lutzemberger, G.; Bertei, A. Critical comparison of equivalent circuit and physics-based models for lithium-ion batteries: A graphite/lithium-iron-phosphate case study. *J. Energy Storage* **2024**, *94*, 112326. [CrossRef]
15. Barzacchi, L.; Lagnoni, M.; Rienzo, R.D.; Bertei, A.; Baronti, F. Enabling early detection of lithium-ion battery degradation by linking electrochemical properties to equivalent circuit model parameters. *J. Energy Storage* **2022**, *50*, 104213. [CrossRef]
16. Watrin, N.; Blunier, B.; Miraoui, A. Review of adaptive systems for lithium batteries State-of-Charge and State-of-Health estimation, 2012. In Proceedings of the IEEE Transportation Electrification Conference and Expo (ITEEC), Dearborn, MI, USA, 18–20 June 2012.

17. He, H.; Xiong, R.; Guo, H.; Li, S. Comparison study on the battery models used for the energy management of batteries in electric vehicles. *Energy Convers. Manag.* **2012**, *64*, 113–121. [CrossRef]

18. Hannan, M.; Lipu, M.; Hussain, A.; Mohamed, A. A review of lithium-ion battery state of charge estimation and management system in electric vehicle applications: Challenges and recommendations. *Renew. Sustain. Energy Rev.* **2017**, *78*, 834–854. [CrossRef]

19. Wang, Y.; Tian, J.; Sun, Z.; Wang, L.; Xu, R.; Li, M.; Chen, Z. A comprehensive review of battery modeling and state estimation approaches for advanced battery management systems. *Renew. Sustain. Energy Rev.* **2020**, *131*, 1110015. [CrossRef]

20. Dini, P.; Colicelli, A.; Saponara, S. Review on Modeling and SOC/SOH Estimation of Batteries for Automotive Applications. *Batteries* **2024**, *10*, 34. [CrossRef]

21. Ali, M.U.; Zafar, A.; Nengroo, S.H.; Hussain, S.; Alvi, M.J.; Kim, H.J. Towards a Smarter Battery Management System for Electric Vehicle Applications: A Critical Review of Lithium-Ion Battery State of Charge Estimation. *Energies* **2019**, *12*, 446. [CrossRef]

22. Movassagh, K.; Raihan, A.; Balasingam, B.; Pattipati, K. A Critical Look at Coulomb Counting Approach for State of Charge Estimation in Batteries. *Energies* **2021**, *14*, 4074. [CrossRef]

23. Tang, X.; Wang, Y.; Chen, Z. A method for state-of-charge estimation of LiFePO4 batteries based on a dual-circuit state observer. *J. Power Sources* **2015**, *296*, 23–29. [CrossRef]

24. Plett, G.L. Extended Kalman filtering for battery management systems of LiPB-based HEV battery packs: Part 1. Background. *J. Power Sources* **2004**, *134*, 252–261. [CrossRef]

25. Plett, G.L. Extended Kalman filtering for battery management systems of LiPB-based HEV battery packs: Part 2. Modeling and identification. *J. Power Sources* **2004**, *134*, 262–276. [CrossRef]

26. Plett, G.L. Extended Kalman filtering for battery management systems of LiPB-based HEV battery packs: Part 3. State and parameter estimation. *J. Power Sources* **2004**, *134*, 277–292. [CrossRef]

27. Plett, G.L. Sigma-point Kalman filtering for battery management systems of LiPB-based HEV battery packs. Part 1: Introduction and state estimation. *J. Power Sources* **2006**, *161*, 1356–1368. [CrossRef]

28. Plett, G.L. Sigma-point Kalman filtering for battery management systems of LiPB-based HEV battery packs. Part 2: Simultaneous state and parameter estimation. *J. Power Sources* **2006**, *161*, 1369–1384. [CrossRef]

29. Kollmeyer, P.; Vidal, C.; Naguib, M.; Skells, M. LG 18650HG2 Li-Ion Battery Data and Example Deep Neural Network xEV SOC Estimator Script, 2020. Mendeley Data V3. Available online: https://data.mendeley.com/datasets/cp3473x7xv/3 (accessed on 2 November 2024).